

## RESEARCH ARTICLE

# A High Angular Stability, Single-Layer Transmission Linear-to-Circular Polarization Converter for Dual ISM-Band Operation

TUNG-LAM VU<sup>ID</sup>, (Student Member, IEEE), AND CHULHUN SEO<sup>ID</sup>, (Senior Member, IEEE)

Department of Information and Communication Convergence, Soongsil University, Dongjak-gu, Seoul 06978, South Korea

Corresponding author: Chulhun Seo (chulhun@ssu.ac.kr)

This work was supported by the Basic Science Research Program at the National Research Foundation of Korea (NRF), funded by the Ministry of Science and the Information and Communications Technology (ICT), under Grant NRF-2017R1A5A1015596.

**ABSTRACT** This paper presents a planar metasurface structure for linear to circular polarization (CP) conversion at the industrial, scientific, and medical bands of 2.4 GHz and 5.8 GHz. The new unit-cell structure consists of two loaded symmetric cross-shaped stubs with a size of  $0.26 \lambda \times 0.26 \lambda$  in a single thin substrate with a thickness of  $0.0064 \lambda$ . The design process and parametric study are presented to clarify the operating mechanism for each frequency. The unit-cell element is analyzed and simulated, which exhibits an axial ratio (AR) bandwidth of 15.8% and 12.6% at a 3-dB criterion with the same polarization mode at 2.4 GHz and 5.8 GHz, respectively. The proposed LP-to-CP converter achieves a stable AR bandwidth with an oblique incident angle up to  $45^\circ$ . Moreover, a dual-band linear polarization (LP) antenna is combined with an array of  $4 \times 4$  unit cells to validate the polarization converting ability of the proposed metasurface. The LP-to-CP converter and the antenna are fabricated and measured. The measurement results show that the antenna obtains a good impedance matching and CP waves radiation at 2.33–2.51 GHz and 5.55–5.89 GHz. The integrated antenna with dual-band CP waves radiation is suitable for improving the transmission efficiency in communication and wireless power transfer applications.

**INDEX TERMS** Dual-band antenna, linear-to-circular converter, metasurface, polarization converter.

## I. INTRODUCTION

Electromagnetic waves with circular polarization (CP) have been widely used in RF signal transceivers since their advantageous properties [1], [2]. They overcome the weaknesses of linear polarization (LP) waves, such as multipath fading and polarization mismatch loss, which is necessary for communication applications. Several antenna structures were proposed for the CP wave achievement, such as coplanar waveguide (CPW)-fed planar antennas [3], cross-dipole antenna [4], substrate integrated waveguide (SIW) cavity [5], antenna array with sequential-phase (SP) [6]. However, designing an antenna with dual-band CP waves remains a challenge by the complex structure of the feeding network [7], [8]. The metasurface as a polarization converter

has emerged as an efficient technique for obtaining CP characteristics from the LP incident wave. The dual-band LP antenna integrated with an LP-to-CP converter can generate dual-band CP waves radiation without the feeding network structures.

Recently, many studies about the LP-to-CP converter at a single or dual-band of Ku-/Ka-band for millimeter-wave and satellite communication applications have been reported in [9], [10], [11], [16]. The polarization converter is divided into two main categories: reflection polarization converter and transmission polarization converter. The transmission LP-to-CP converter is based on meander lines (ML) [17], Jerusalem cross (JC) [18], split-ring-based (SPR) [19] structures with single band operation. In contrast, the dual-band LP-to-CP converter is designed in multi-substrates [20], [21], making a bulky structure, increasing the dimensions and fabrication difficulty. The simple transmission polarization

The associate editor coordinating the review of this manuscript and approving it for publication was Bilal Khawaja<sup>ID</sup>.

**TABLE 1. Comparison of the proposed unit cell with related works.**

Reference	Frequency (GHz)	Structure	Dimensions ( $\lambda$ )	Metallic layers	AR BW (%)	Angular stability	Polarization mode
[10]	20.67 29.71	SPR	$0.27 \times 0.27 \times 0.1$	2	5.56 3.97	$45^\circ$	Orthogonal
[11]	18.5 29	JC	$0.25 \times 0.25 \times 0.1$	2	29 12	$20^\circ$	Orthogonal
[12]	19.95 29.75	SPR	$0.35 \times 0.35 \times 0.07$	3	2.5 1.7	$30^\circ$	Orthogonal
[18]	17.8 36.5	SQR & SPR	$0.32 \times 0.32 \times 0.017$	2	25 16.4	–	Orthogonal
[19]	17.2 34.2	SQR & SPR	$0.32 \times 0.32 \times 0.017$	1	21.3 21.2	$45^\circ$	Orthogonal
[26]	15.1 16.5	SPR	$0.4 \times 0.4 \times 0.4$	2	11.8 6.9	–	Same
[27]	7.6 13	SPR	$0.22 \times 0.23 \times 0.24$	4	31 13.8	$25^\circ$	Same
This work	2.4 5.8	CS	$0.26 \times 0.26 \times 0.0064$	1	15.8 12.6	$45^\circ$	Same

$\lambda$ : wavelength at lower frequency, BW: Bandwidth, – :not mentioned.  
SPR: Split-ring, SQR: Square ring, JC: Jerusalem cross, CS: Cross-shaped.

converters have been proposed in [12], [13], and [22]. The unit-cell structure consists of a split ring or squares arranged inside a square ring to obtain dual/tri-band operation in an ultra-thin substrate. On the other hand, the reflection polarization converters with a similar structure and a ground layer for reflecting incident waves can achieve high angular stability and a larger axial ratio (AR) bandwidth than the transmission polarization converters, as reported in [23] and [24]. However, the transmission polarization converters are usually integrated with the antenna using a periodic structure to generate the CP wave radiation, which makes it more convenient to design the low-profile CP integrated antenna.

Wireless power transfer (WPT) is a potential technique for charging devices based on the energy of the electromagnetic wave. With the CP wave, the efficiency of the WPT system is significantly improved in case of misalignment between transmitter and receiver, ensuring energy-supplying stability for systems [25]. The WPT system mainly operates in the ISM bands, typically at 2.4 GHz and 5.8 GHz, for communication and power transfer. In the WPT systems deployed simultaneously for data transmission and power transfer at these bands, the transmitter antenna with the CP waves will enhance the transmission efficiency for both applications. In [26], the antenna combined with an LP-to-CP converter metasurface achieves CP radiation at a single band of 2.45 GHz. The unit-cell structure is a rectangular loop with a diagonal microstrip. Especially in [27], the low-profile CP metasurface-based bowtie slot antenna has AR broadband characteristic of 31.7% (4.38–5.98 GHz), but insufficient for both the ISM bands at 2.4 GHz and 5.8 GHz due to their large band gap.

In this paper, a transmission LP-to-CP converter is designed and analyzed. The unit-cell structure is based on two symmetric cross-shaped stubs loaded on a single thin substrate. The designing steps and parametric results explain the operating mechanism of the structure for each frequency. The polarization converter operates at the dual ISM bands

of 2.4 GHz and 5.8 GHz with AR bandwidths of 15.8% and 12.6%, respectively. Table 1 compares the proposed polarization converter with the recent related studies on dimensions, operating frequency, number of layers, AR bandwidth, and angular stability. It can be seen that the proposed unit-cell structure has advantages in simple structure, just a single metallic layer in the substrate, it is easy for fabrication. Besides the small size of  $0.26\lambda$ , the high angular stability of  $45^\circ$  and the thickness of the substrate (calculated in  $\lambda$ ) is much thinner than other structures, it easily integrates with the antenna to obtain CP wave radiation as a low-profile antenna. The AR bandwidths are over 10% at both bands, which is not broad AR bandwidth as [15] and [13], but wide enough according to the frequency allocations standard for ISM bands of 2.4–2.5 GHz and 5.725–5.825 GHz. In addition, a simple dual-band LP antenna with the same frequency is used to verify the polarization-converting ability of the converter. As a result, the antenna obtains the simultaneous CP radiation waves at 2.33–2.51 GHz and 5.55–5.89 GHz. The simulation and measurement results exhibit a good agreement. This design is a potential candidate for efficiency enhancement in dual-band WPT and communication systems.

## II. DUAL-BAND LINEAR TO CIRCULAR POLARIZATION CONVERTER DESIGN

### A. BRIEF REVIEW OF POLARIZATION CONVERTER PRINCIPLE

An incident electric field  $E^i$  consisting of two components in  $E_x^i$  and  $E_y^i$ , is expressed as follows:

$$\vec{E}^i = \hat{x}E_x^ie^{jkz} + \hat{y}E_y^ie^{jkz} \quad (1)$$

When the incident wave goes through the metasurface, transmission matrix  $T$  represents the relation between complex

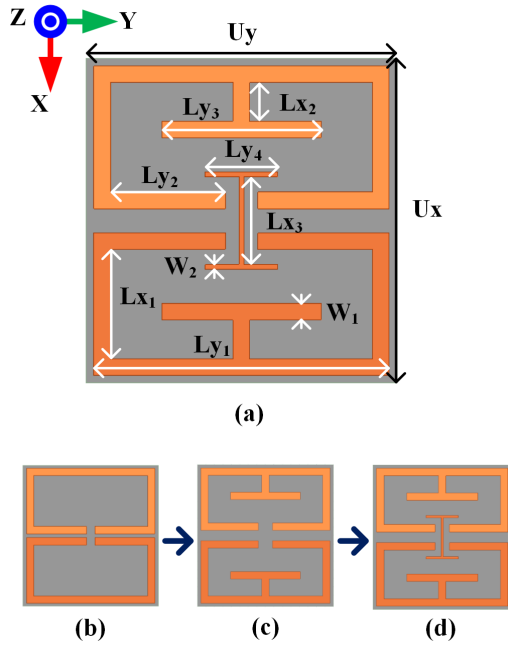


FIGURE 1. The proposed unit cell and design steps: (a) Geometry of the unit cell, (b) Step 1, (c) Step 2, and (d) Step 3.

amplitudes of incident and transmission field.

$$\begin{bmatrix} E_x^t \\ E_y^t \end{bmatrix} = \begin{bmatrix} T_{xx} & T_{xy} \\ T_{yx} & T_{yy} \end{bmatrix} \begin{bmatrix} E_x^i \\ E_y^i \end{bmatrix} \quad (2)$$

where the cross-transmission coefficients  $T_{xy}$  and  $T_{yx}$  are nearly zero due to the weak coupling of two orthogonal components [10]. Therefore,  $T_{xx}$  and  $T_{yy}$  are shown as the polarization transmission coefficients and are derived as:

$$T_{xx} = |T_{xx}|e^{j\phi_{xx}}, T_{yy} = |T_{yy}|e^{j\phi_{yy}} \quad (3)$$

Furthermore, the phase difference between the two components is given by:  $\Delta\phi = \phi_{yy} - \phi_{xx}$ . To achieve the CP wave, the magnitudes and phases of the transmission coefficient should be satisfied the final condition:

$$\begin{cases} |T_{xx}| = |T_{yy}| \\ \Delta\phi = \pm \frac{\pi}{2} \end{cases} \quad (4)$$

Consequently, the AR parameter given by [10]:

$$AR = \sqrt{\frac{|T_{xx}|^2 + |T_{yy}|^2 + \sqrt{p}}{|T_{xx}|^2 + |T_{yy}|^2 - \sqrt{p}}} \quad (5)$$

where  $p = |T_{xx}|^4 + |T_{yy}|^4 + 2|T_{xx}|^2|T_{yy}|^2 \cos(2\Delta\phi)$ , which is derived based on the transmission coefficient amplitudes and phases difference. As a result, the AR parameter value below the 3-dB should be obtained at the desired operating frequency to achieve the CP characteristics. The phase difference of  $\frac{\pi}{2}$  or  $-\frac{\pi}{2}$  defines the polarization mode of the CP wave are right-handed circular polarization (RHCP) or left-handed circular polarization (LHCP), respectively.

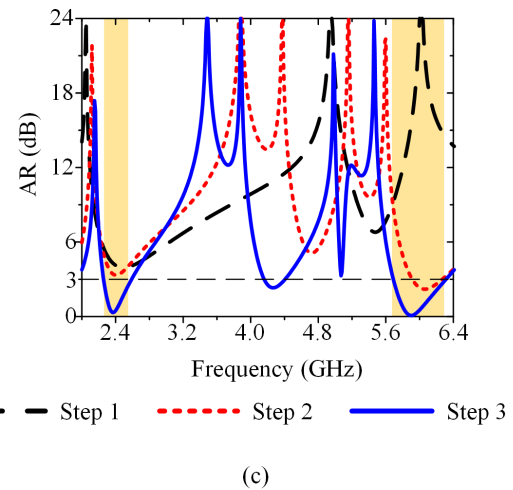
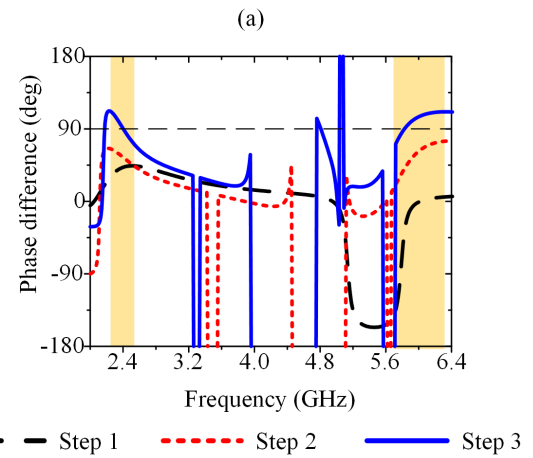
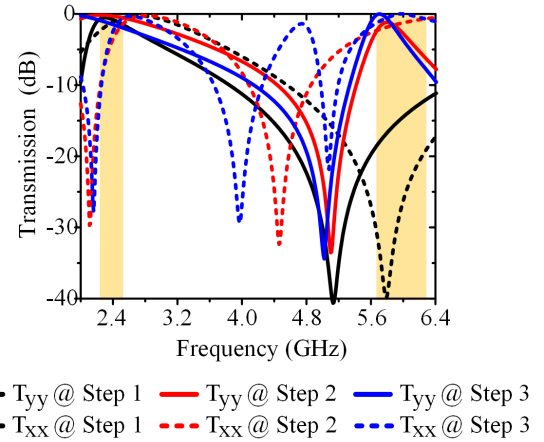
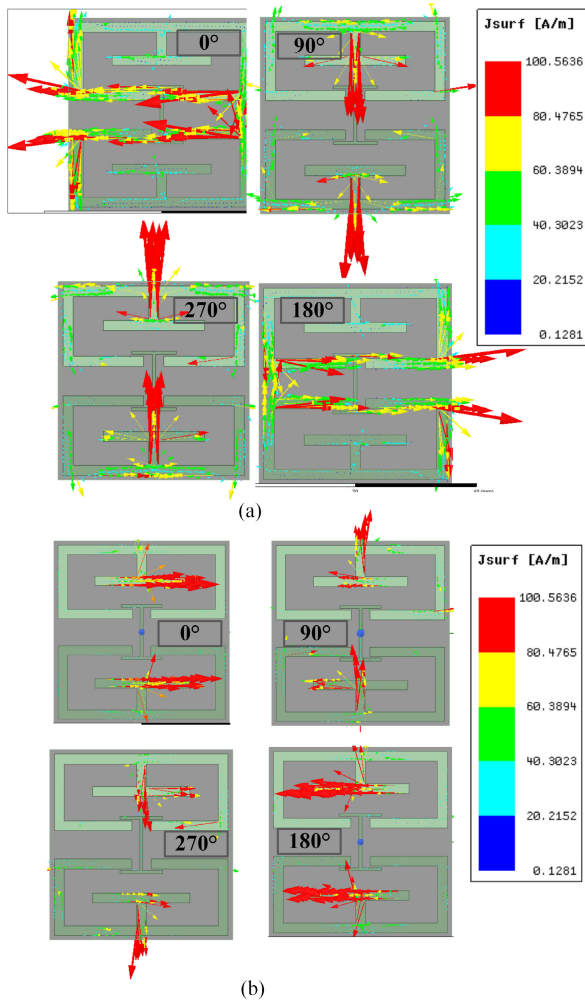


FIGURE 2. The comparison of design steps: (a) Transmission coefficient, (b) Phase difference, and (c) AR value.

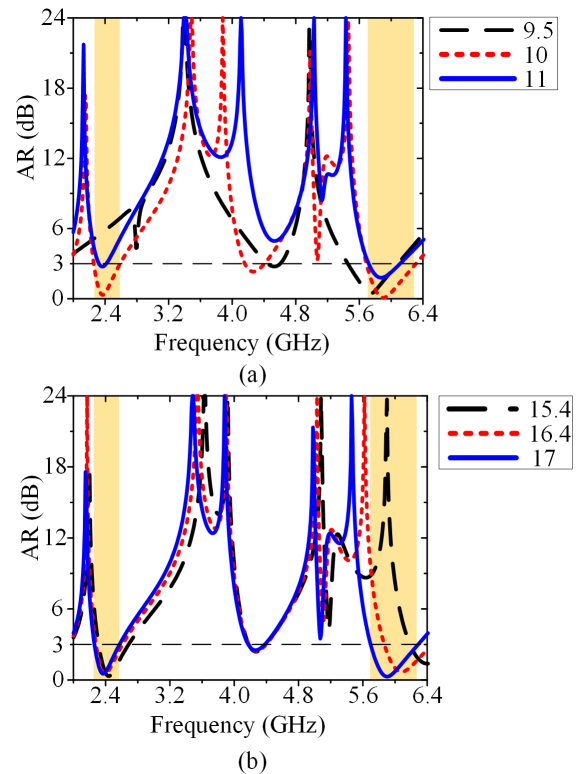
B. GEOMETRY OF THE UNIT CELL

Fig. 1 illustrates the proposed unit cell configuration. The unit cell is configured on a single layer of FR4-epoxy substrate ( $\epsilon_r = 4.4$  and  $\tan\delta = 0.002$ ) with an overall dimension of



**FIGURE 3.** The surface distribution current at the resonant frequency: (a) 2.4 GHz, (b) 5.8 GHz.

33.2 mm × 32 mm × 0.8 mm (0.26λ × 0.26λ × 0.0064λ, λ is the wavelength at 2.4 GHz). In the design of unit cells, the impedance manipulates the phase or group velocity to control surface waves. The unit-cell size smaller than the wavelength can be easily expressed in terms of homogeneity boundary conditions of impedance; it is related to the tangential components of the average electric and magnetic fields [28]. The symmetric geometry comprises two cross-shaped stubs loaded with an I-shape in the center. The symmetric geometry to prevent cross-coupling between the electric field components along the x- and y-direction [9]. The cross-shaped stubs generate resonances at dual-band, and I-shape in the center adjusts the phase difference to improve the AR. The properties of the unit cell are simulated in Ansys HFSS with Floquet port and periodic boundary master-slave conditions. The incident wave is transmitted into two directions corresponding x and y-axis. Based on the transmission coefficient and phase difference results, the AR value is calculated following the equation (5).



**FIGURE 4.** The AR value with the variation of the parameter: (a)  $L_{x1}$  (mm), (b)  $L_{y3}$  (mm).

**C. DESIGN EVOLUTION AND PARAMETRIC ANALYSIS**

Figs. 1(b)–(d) demonstrate the evolution of the unit cell by modifying the cross-shaped stubs loaded structure from single-band resonance at step 1, dual-band resonance at step 2, and increasing the phase difference to satisfy CP conditions in the final step. The transmission coefficient, phase difference, and AR value of the unit cell in each step are shown in Figs. 2(a)–(c). In more detail, in step 1, the unit cell operates at a single-band of 2.4 GHz with a transmission coefficient higher than -1.5 dB for both x and y-directions and the phase difference of around 40°. Step 2, adding the T-shape, generates one more resonant frequency at 5.8 GHz, as shown in the transmission coefficient in Fig. 2(a). However, the AR values at dual-band are still higher than 3 dB because the phase difference is insufficient 90°. By adding the I-shape in step 3, the phase difference in both bands is increased at around 90° as shown in Fig. 2(b). Besides, the transmission coefficient at 5.8 GHz is improved higher than -1 dB. Herein, the AR values below 3 dB as shown in Fig. 2(c). The transmission magnitudes of  $T_{xx}$  and  $T_{yy}$  at 2.4 GHz and 5.8 GHz are nearly same, the phase difference is approximately 90 degrees, and it satisfies the CP conditions as the equation (4).

The surface current distribution on the metallic surface in Fig. 3 verifies the results of the design steps. At 2.4 GHz, the surface current concentrates on the outer line corresponding to the structure in step 1. In contrast, the surface current at

**TABLE 2.** Parameter value of the proposed unit cell.

Parameter	Value (mm)	Parameter	Value (mm)	Parameter	Value (mm)
$U_x$	33.3	$Ly_1$	30.35	$Lx_1$	10
$U_y$	32	$Ly_2$	12.8	$Lx_2$	4
$W_1$	1.7	$Ly_3$	17	$Lx_2$	9
$W_2$	2.5	$Ly_4$	7.45		

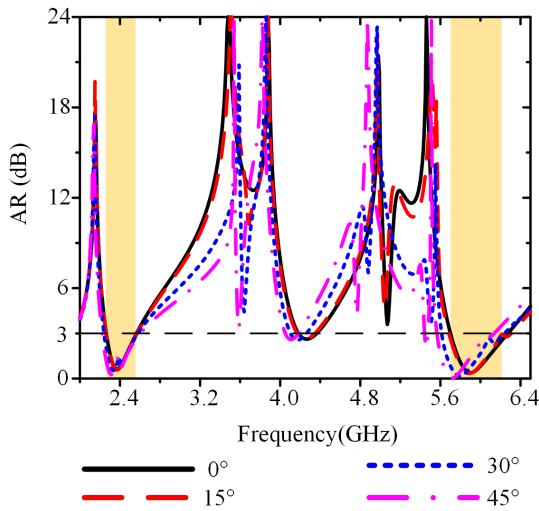


**FIGURE 5.** Simulated AR at different incident angles.

5.8 GHz is mainly on the T-shape added in step 2, as shown in Fig. 3(b). It is good evidence to show that the unit cell can operate at dual-band by cross-shaped stubs. Additionally, the orientation of the surface current at dual-band with different phases ( $0^\circ$ ,  $90^\circ$ ,  $180^\circ$ , and  $270^\circ$ ) are shown in Fig. 3 to demonstrate the CP operation mechanism. It can be observed that the surface current with anti-clockwise rotation at both resonance frequencies creates RHCP wave radiation. The similarity in polarization mode at dual-band is also shown by the same phase difference  $90^\circ$  in Fig. 2(b).

The  $Lx_1$  and  $Ly_3$  are the lengths in part of the structure where the surface distribution currents are concentrated. Fig. 4 shows the AR value results according to the variation of these parameters. The AR value has significantly been affected by changing  $Lx_1$ , even is vanished the CP at 2.4 GHz with a length of 9.5 mm, as shown in Fig. 4(a). However, it does not affect the AR value at 5.8 GHz frequency much. In contrast, the AR value is stable at 2.4 GHz by varying the parameter  $Ly_3$ , but it is shifted to the higher frequency around the 5.8 GHz band if the length of  $Ly_3$  is reduced, as shown in Fig. 4(b). It can be seen that the adjusting  $Lx_1$  and  $Ly_3$  individual affect AR values at 2.4 GHz and 5.8 GHz, respectively.

Table 2 presents the final optimized parameters, ensuring that the unit cell operates with AR less than 3 dB at the dual

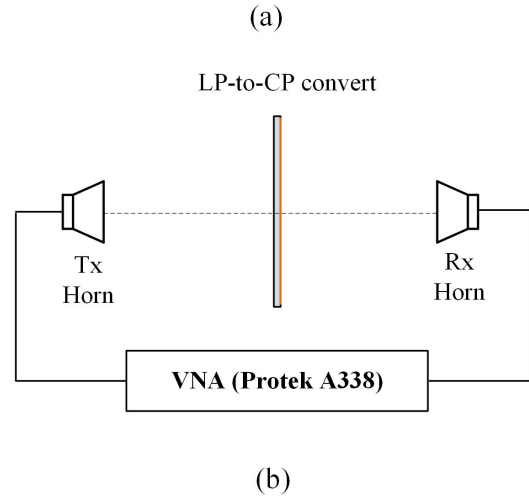
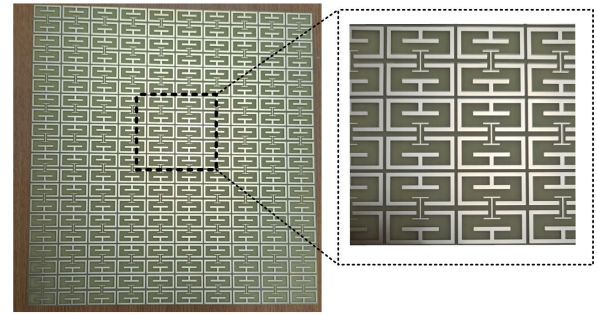


**FIGURE 6.** Measurement of the array LP-to-CP converter: (a) The array of  $10 \times 10$  elements LP-to-CP converter, (b) Measurement setup.

ISM bands. The proposed polarization converter achieves the CP operation at 2.4 GHz and 5.8 GHz and 3 dB AR bandwidth of 15.8% (2.25–2.63 GHz) and 12.6% (5.67–6.4 GHz). The incident wave from the radiation antenna is an oblique incident wave. Therefore, the AR values are investigated with different incident angles from  $0^\circ$  to  $45^\circ$ . The angular stability of the proposed converter is shown in Fig. 5. The AR value is observed to be stable with incident angle up to  $45^\circ$ , below 3 dB at both center frequencies, and the AR bandwidth slightly changes at the higher frequency band. As a result, the proposed LP-to-CP converter achieves good angular stability.

### III. FABRICATION AND MEASUREMENT

#### A. EXPERIMENTAL VERIFICATION OF THE PROPOSED DUAL-BAND LP-TO-CP CONVERTER

The fabricated prototype of the proposed LP-to-CP converter metasurface is shown in Fig. 6(a). The array of  $10 \times 10$  unit cell elements is used to validate the polarization converter's properties by direct measurement. The array of  $10 \times 10$  elements of the unit cell is measured with two broadband horn antennas connected to the vector network analyzer (VNA Protek A338), and the measurement setup is shown in Fig. 6(b). The horn antennas as transmitting and receiving antennas have been placed on both sides of the

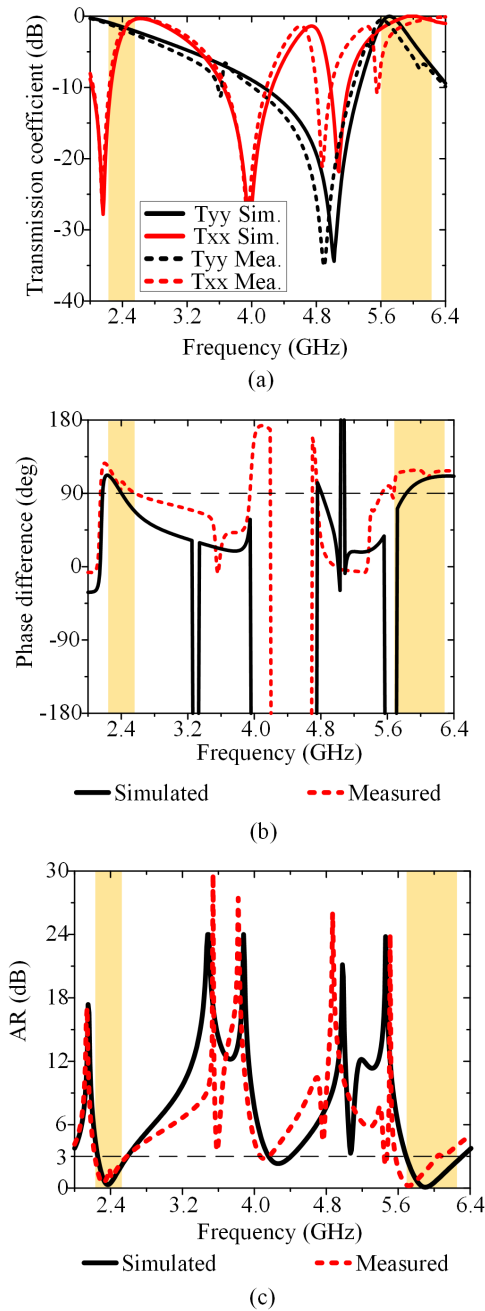


**FIGURE 7.** Measurement results of the array of  $10 \times 10$  elements LP-to-CP converter: (a) Transmission coefficient, (b) Phase difference, and (c) AR value.

metasurface to investigate the transmission coefficient and phase difference corresponding to the x and y- directions. The polarization converter is placed in the far-field region of the antenna to obtain the exact measurement results [23]. The measurement results of the array of  $10 \times 10$  elements LP-to-CP converter in Figs. 7(a)-(c) show the transmission coefficients, phase difference, and AR value. A good agreement between the measured and simulated transmission coefficients, whereas the phase difference has a slight difference of  $10^\circ - 30^\circ$  with the simulation result. However,

**TABLE 3.** Simulated result analysis for the different array of unit cell.

Array	Distance (mm)	$S_{11}$ (dB)		AR (dB)	
		2.4 GHz	5.8 GHz	2.4 GHz	5.8 GHz
$3 \times 3$	34.7	-11.3	-15.4	4.4	6.3
$4 \times 4$	31.5	-16.6	-16.9	1.6	1.4
$5 \times 5$	32.2	-17.1	-18.5	1.8	2.1
$6 \times 6$	36.35	-16.9	-20.4	2.4	1.6
$8 \times 8$	41.05	-15.3	-15.8	2.1	2.2
$10 \times 10$	47.1	-16.2	-14.5	2.35	1.7

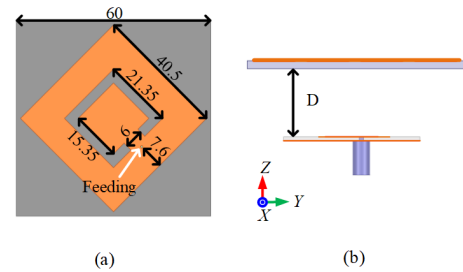


**FIGURE 8.** The dual-band antenna with metasurface: (a) Geometry of the antenna, (b) Configuration of the antenna with metasurface. The units are in millimeters.

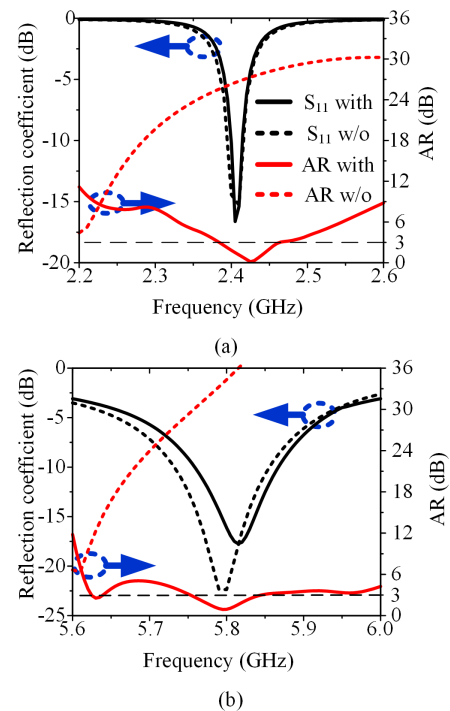


**FIGURE 9.** Reflection coefficient and AR value of the antenna with and without the LP-to-CP converter at: (a) 2.4 GHz, (b) 5.8 GHz.

the AR values at the center of the two desired frequencies are 1.39 dB and 0.7 dB, acceptable by less than 3 dB, and shown in more detail in Fig. 7(c). The difference between the measurement and simulation results by the simulation results assume an infinite number of unit-cell elements. In contrast, the number of the unit-cell array is fixed in measurement.

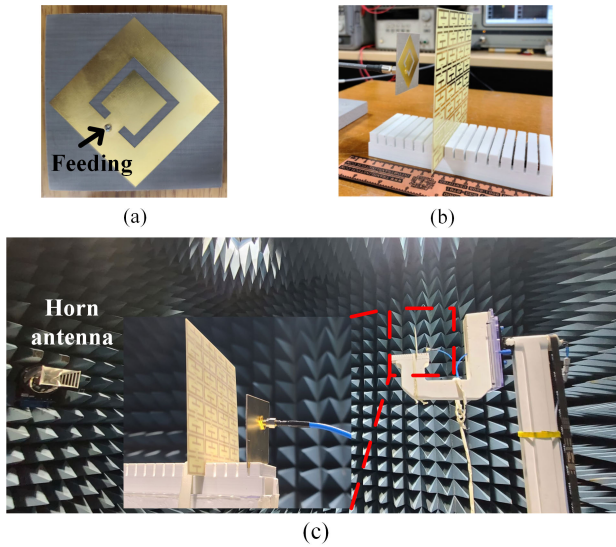


**FIGURE 10.** Fabrication and measurement: (a) LP dual-band antenna, (b) The integrated antenna with LP-to-CP converter, and (c) Measurement the antenna with the array of  $4 \times 4$  metasurface in chamber room.

**B. THE INTEGRATED DUAL-BAND ANTENNA WITH LP-TO-CP CONVERTER**

In order to verify the polarization converting ability in cases integrated with the antenna, an LP dual-band antenna has been implemented. The dual-band antenna is designed on the TLY-5 substrate ( $\epsilon_r = 2.2$  and  $\tan\delta = 0.0009$ ) with a thickness of 1.2 mm. The dimensions and the configuration of the polarization converter with the antenna are shown in Fig. 8. The polarization converter metasurface is placed in the radiation region of the antenna with a distance greater than  $\lambda/4$ . The simulated result for the different arrays of the unit cell with optimal distance is illustrated in Table 3. It can be seen that, the array of  $4 \times 4$  elements of the unit cell with a distance of 31.5 mm yields the best results of AR value, which are 1.6 dB and 1.4 dB at 2.4 GHz and 5.8 GHz, respectively. Besides, the antenna also achieves an AR value of less than 3 dB at dual-band in case the array of unit cell with a larger number of elements. The simulation results of the reflection coefficient and the AR value of the dual-band antenna are illustrated in Fig. 9. The antenna operates well at the dual ISM bands of 2.4 GHz and 5.8 GHz with a reflection coefficient of less than -10 dB at the frequency bands 2.38–2.43 GHz and 5.72–5.87 GHz. The AR value of 26.3 dB and 34.4 dB at two center frequencies. With the proposed LP-to-CP converter, the reflection coefficient changes negligibly, and the CP wave radiation is achieved at both bands with the AR bandwidth of 2.38–2.46 GHz and 5.75–5.85 GHz.

The LP antenna with the  $4 \times 4$  metasurface polarization converter array is measured in a microwave chamber, shown in Fig. 10. Fig. 11 illustrates the antenna’s reflection coefficient and polarization properties. It can be seen that the antenna operates exactly at dual-band. The difference between the measurement and simulation results of the

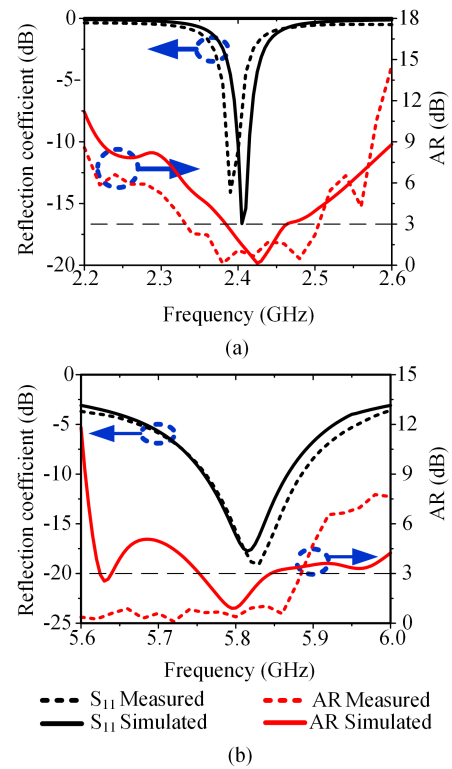


**FIGURE 11.** Reflection coefficient and AR value at: (a) 2.4 GHz, (b) 5.8 GHz.

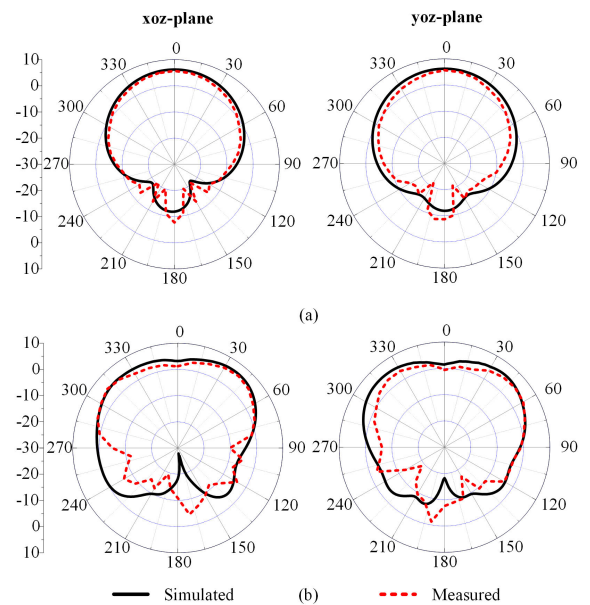


**FIGURE 12.** The simulated and measured radiation patterns of the LP antenna at: (a) 2.4 GHz, (b) 5.8 GHz.

reflection coefficient is negligible. Fig. 12 shows the radiation patterns of the antenna without the polarization converter. With the polarization converter, the antenna achieves the CP wave radiation at the ISM bands of 2.4 GHz and 5.8 GHz, as demonstrated in the AR values of 1.39 dB and

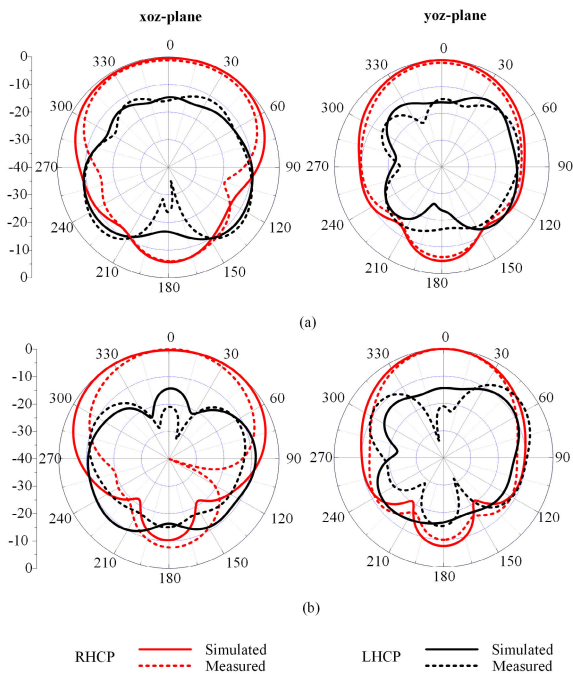


**FIGURE 13.** The simulated and measured radiation patterns of the antenna with the LP-to-CP converter at: (a) 2.4 GHz, (b) 5.8 GHz.

0.68 dB with the AR bandwidth of 2.33–2.51 GHz (7.5%) and 5.55–5.89 GHz (5.9%), respectively. Fig. 13 illustrates the measured and simulated radiation patterns at two center frequencies in the xoz and yoz-planes. The radiation patterns are broadside in each plane, and the RHCP radiation is greater than the LHCP radiation by about 13 dB at 2.4 GHz and about 20 dB at 5.8 GHz. Hence, the integrated antenna with the proposed LP-to-CP converter easily generates dual-band CP waves radiation without the complex feeding network. With both experimental verification methods and the results are shown in Fig. 7 and Fig. 11, it can be seen that the proposed LP-to-CP converter operates accurately and can convert the LP wave to CP wave radiation at dual ISM bands. The CP wave radiation at dual ISM bands can improve the transmission efficiency in communication and WPT applications.

#### IV. CONCLUSION

The dual-band transmission LP-to-CP converter is proposed in this paper, which consists of two symmetric cross-shaped stubs loaded in a layer with unit-cell dimensions of  $0.26\lambda \times 0.26\lambda \times 0.0064\lambda$  ( $\lambda$  is the wavelength at 2.4 GHz). The designing steps and parametric study are analyzed in detail to clarify the operating mechanism for each frequency. The polarization converter operates at the dual ISM bands of 2.4 GHz and 5.8 GHz with the similarity in polarization mode (RHCP). The angular stability are  $45^\circ$  and the AR bandwidths are 15.8% (2.25–2.63 GHz) and 12.6% (5.67–6.4 GHz). The proposed converter has advantages in simple structure, and it is easy for fabrication. The LP dual-band antenna combined with the metasurface achieves the CP radiation wave at

dual-band, and the measured AR bandwidth at below 3 dB is 2.33–2.51 GHz and 5.55–5.89 GHz. This polarization converter is useful for communication and WPT applications.

#### REFERENCES

- [1] Y. He, C. Gu, H. Ma, J. Zhu, and G. V. Eleftheriades, "Miniaturized circularly polarized Doppler radar for human vital sign detection," *IEEE Trans. Antennas Propag.*, vol. 67, no. 11, pp. 7022–7030, Nov. 2019.
- [2] C. Shu, J. Wang, S. Hu, Y. Yao, and J. Yu, "A wideband dual-circular-polarization horn antenna for mmWave wireless communications," *IEEE Antennas Wireless Propag. Lett.*, vol. 18, no. 9, pp. 1726–1730, Sep. 2019.
- [3] S. Ahdi Rezaeieh, A. Abbosh, and M. A. Antoniades, "Compact CPW-fed planar monopole antenna with wide circular polarization bandwidth," *IEEE Antennas Wireless Propag. Lett.*, vol. 12, pp. 1295–1298, 2013.
- [4] Y. He, W. He, and H. Wong, "A wideband circularly polarized cross-dipole antenna," *IEEE Antennas Wireless Propag. Lett.*, vol. 13, pp. 67–70, 2014.
- [5] S. Priya, K. Kumar, S. Dwari, and M. K. Mandal, "Circularly polarized self-diplexing SIW cavity backed slot antennas," *IEEE Trans. Antennas Propag.*, vol. 68, no. 3, pp. 2387–2392, Mar. 2020.
- [6] S. X. Ta and I. Park, "Compact wideband circularly polarized patch antenna array using metasurface," *IEEE Antennas Wireless Propag. Lett.*, vol. 16, pp. 1932–1936, 2017.
- [7] J.-D. Zhang, W. Wu, and D.-G. Fang, "Dual-band and dual-circularly polarized shared-aperture array antennas with single-layer substrate," *IEEE Trans. Antennas Propag.*, vol. 64, no. 1, pp. 109–116, Jan. 2016.
- [8] C.-X. Mao, S. Gao, Y. Wang, Q.-X. Chu, and X.-X. Yang, "Dual-band circularly polarized shared-aperture array for C-/X-band satellite communications," *IEEE Trans. Antennas Propag.*, vol. 65, no. 10, pp. 5171–5178, Oct. 2017.
- [9] M. A. Sofi, K. Saurav, and S. K. Koul, "Frequency-selective surface-based compact single substrate layer dual-band transmission-type linear-to-circular polarization converter," *IEEE Trans. Microw. Theory Techn.*, vol. 68, no. 10, pp. 4138–4149, Oct. 2020.
- [10] H. B. Wang and Y. J. Cheng, "Single-layer dual-band linear-to-circular polarization converter with wide axial ratio bandwidth and different polarization modes," *IEEE Trans. Antennas Propag.*, vol. 67, no. 6, pp. 4296–4301, Jun. 2019.
- [11] P. Naseri, S. A. Matos, J. R. Costa, C. A. Fernandes, and N. J. G. Fonseca, "Dual-band dual-linear-to-circular polarization converter in transmission mode application to K/Ka-band satellite communications," *IEEE Trans. Antennas Propag.*, vol. 66, no. 12, pp. 7128–7137, Dec. 2018.
- [12] A. K. Fahad, C. Ruan, R. Nazir, T. U. Haq, and W. He, "Dual-band ultrathin meta-array for polarization conversion in Ku/Ka-band with broadband transmission," *IEEE Antennas Wireless Propag. Lett.*, vol. 19, no. 5, pp. 856–860, May 2020.
- [13] A. K. Fahad, C. Ruan, R. Nazir, M. Saleem, T. U. Haq, S. Ullah, and W. He, "Ultra-thin metasheet for dual-wide-band linear to circular polarization conversion with wide-angle performance," *IEEE Access*, vol. 8, pp. 163244–163254, 2020.
- [14] F. A. Mangi, S. Xiao, Z. Yao, I. Memon, and G. F. Kakepoto, "Dual-band asymmetric circular polariser based on fission transmission of linearly polarised wave," *IET Microw., Antennas Propag.*, vol. 12, no. 8, pp. 1414–1419, 2018.
- [15] Q. Zeng, W. Ren, H. Zhao, Z. Xue, and W. Li, "Dual-band transmission-type circular polariser based on frequency selective surfaces," *IET Microw., Antennas Propag.*, vol. 13, no. 2, pp. 216–222, Feb. 2019.
- [16] H. B. Wang, Y. J. Cheng, and Z. N. Chen, "Dual-band miniaturized linear-to-circular metasurface polarization converter with wideband and wide-angle axial ratio," *IEEE Trans. Antennas Propag.*, vol. 69, no. 12, pp. 9021–9025, Dec. 2021.
- [17] P. Fei, Z. Shen, X. Wen, and F. Nian, "A single-layer circular polarizer based on hybrid meander line and loop configuration," *IEEE Trans. Antennas Propag.*, vol. 63, no. 10, pp. 4609–4614, Oct. 2015.
- [18] M. Hosseini and S. V. Hum, "A circuit-driven design methodology for a circular polarizer based on modified Jerusalem cross grids," *IEEE Trans. Antennas Propag.*, vol. 65, no. 10, pp. 5322–5331, Oct. 2017.
- [19] M. Eular, V. Fusco, R. Cahill, and R. Dickie, "325 GHz single layer sub-millimeter wave FSS based split slot ring linear to circular polarization converter," *IEEE Trans. Antennas Propag.*, vol. 58, no. 7, pp. 2457–2459, Jul. 2010.



- [20] W. Zhang, J.-Y. Li, and J. Xie, "A broadband circular polarizer based on cross-shaped composite frequency selective surfaces," *IEEE Trans. Antennas Propag.*, vol. 65, no. 10, pp. 5623–5627, Oct. 2017.
- [21] L. Martinez-Lopez, J. Rodriguez-Cuevas, J. I. Martinez-Lopez, and A. E. Martynyuk, "A multilayer circular polarizer based on bisected splitting frequency selective surfaces," *IEEE Antennas Wireless Propag. Lett.*, vol. 13, pp. 153–156, 2014.
- [22] A. K. Fahad, C. Ruan, S. A. K. M. Ali, R. Nazir, T. U. Haq, S. Ullah, and W. He, "Triband ultrathin polarization converter for X/Ku/Ka-band microwave transmission," *IEEE Microw. Wireless Compon. Lett.*, vol. 30, no. 4, pp. 351–354, Apr. 2020.
- [23] X. Liu, Y. Zhou, C. Wang, L. Gan, X. Yang, and L. Sun, "Dual-band dual-rotational-direction angular stable linear-to-circular polarization converter," *IEEE Trans. Antennas Propag.*, vol. 70, no. 7, pp. 6054–6059, Jul. 2022.
- [24] B. Kamal, J. Chen, Y. Yin, J. Ren, S. Ullah, and U. Ali, "Design and experimental analysis of dual-band polarization converting metasurface," *IEEE Antennas Wireless Propag. Lett.*, vol. 20, no. 8, pp. 1409–1413, Aug. 2021.
- [25] D. M. Nguyen, N. D. Au, and C. Seo, "A microwave power transmission system using sequential phase ring antenna and inverted class F rectenna," *IEEE Access*, vol. 9, pp. 134163–134173, 2021.
- [26] H. L. Zhu, S. W. Cheung, K. L. Chung, and T. I. Yuk, "Linear-to-circular polarization conversion using metasurface," *IEEE Trans. Antennas Propag.*, vol. 61, no. 9, pp. 4615–4623, Sep. 2013.
- [27] C. H. S. Nkimbeng, H. Wang, and I. Park, "Low-profile wideband unidirectional circularly polarized metasurface-based bowtie slot antenna," *IEEE Access*, vol. 9, pp. 134743–134752, 2021.
- [28] R. Quarfoth and D. Sievenpiper, "Artificial tensor impedance surface waveguides," *IEEE Trans. Antennas Propag.*, vol. 61, no. 7, pp. 3597–3606, Jul. 2013.



**TUNG-LAM VU** (Student Member, IEEE) received the B.S. degree from the School of Electronics and Telecommunication, Hanoi University of Science and Technology, Hanoi, Vietnam, in 2019. He is currently pursuing the Ph.D. degree with the Department of Information and Communication Convergence, Soongsil University, Seoul, South Korea. His current research interests include wireless power transfer, antenna design, implantable antenna, and metamaterials.



**CHULHUN SEO** (Senior Member, IEEE) received the B.S., M.S., and Ph.D. degrees from Seoul National University, Seoul, South Korea, in 1983, 1985, and 1993, respectively. From 1993 to 1995, he was with the Massachusetts Institute of Technology (MIT), Cambridge, MA, USA, as a Technical Staff Member. From 1993 to 1997, he was with Soongsil University, Seoul, as an Assistant Professor. From 1999 to 2001, he was a Visiting Professor with MIT. From 1997 to 2004, he was an

Associate Professor with Soongsil University, where he has been a Professor of electronic engineering, since 2004. He is the President of the Korean Institute of Electromagnetic Engineering and Science (KIEES), the Dean of Information and Telecommunications College, Soongsil University, and the Director of the Wireless Power Transfer Research Center, supported by the Korean Government's Ministry of Trade, Industry, and Energy; the Metamaterials Research Center, supported by Basic Research Laboratories (BRL) through an NRF Grant funded by MSIP; and the Center for Intelligent Biomedical Wireless Power Transfer, supported by the National Research Foundation of Korea (NRF) funded by MSIP. His research interests include wireless technologies, RF power amplifiers, and wireless power transfer using metamaterials. He was the Chairperson of the IEEE MTT Korea Chapter, from 2011 to 2014.

...